Journal of Power Sources 257 (2014) 402–411

Contents lists available at ScienceDirect

Journal of Power Sources

journal homepage: www.elsevier.com/locate/jpowsour

Sensitivity analysis of a mathematical model of lithium–sulfur cells: Part II: Precipitation reaction kinetics and sulfur content

Mahmoudreza Ghaznavi, P. Chen*

Department of Chemical Engineering and Waterloo Institute for Nanotechnology, University of Waterloo, 200 University Avenue West, Waterloo, ON N2L3G1, Canada

HIGHLIGHTS

- The discharge behavior of Li–S cells in wide range of rate constants for precipitation reactions is studied.
- Dissolution of elemental sulfur and precipitation of produced polysulfides play an important role in capacity performance.
- Optimum sulfur content is obtained to maintain the maximum capacity performance.
- Formulating the precipitation reactions and electrochemical reactions is needed to be modified in future works.

ARTICLE INFO

Article history:
Received 8 July 2013
Received in revised form
16 December 2013
Accepted 17 December 2013
Available online 31 January 2014

Keywords:
Lithium–sulfur battery
Modeling battery
Simulations
Cathode conductivity

ABSTRACT

A sensitivity analysis of a mathematical model of a lithium–sulfur (Li–S) battery was performed, focusing on the precipitation rate constants and sulfur content, by investigating the response of the model to the variation of these parameters over a wide mathematical range. The necessity of rapid dissolution of elemental sulfur and rapid precipitation of reduced sulfur is discussed in detail. The sensitivity analysis suggests modifying the reduction reaction steps of sulfur can improve the predictions of the model of Li–S battery. Furthermore, an upper limit on the sulfur content of the cathode exists to ensure optimal performance. Although the model provides valuable knowledge concerning Li–S batteries, a modification to the assumed five-step reduction of sulfur combined with the consideration of the insulating nature of the active material is required to improve the model.

1. Introduction

Sulfur (S) one of the favorite active materials for Lithium (Li) batteries due to its high theoretical specific capacity, low cost, high availability, and non-toxic nature [1]. However, several serious problems hinder the commercialization of rechargeable Li–S batteries. For example, the low electronic conductivity of sulfur and polysulfides necessitates the addition of conductive materials to the cathode, and the dissolution of polysulfides leads to a shuttle mechanism that causes self-discharging of the cell [2,3]. Despite the complex and not fully understood behavior of sulfur [4–6], attempts have been made to simulate Li–S batteries to provide insight into their mechanism of operation [7,8].

Continuing the work of Part I [9], this paper presents a sensitivity analysis of the model presented by K. Kumaresan et al. [8] on precipitation constant rates. The model considers a five-step electrochemical reduction reaction of elemental sulfur and also includes the dissolution and precipitation reactions of sulfur and polysulfides across the cell. However, the authors introduced numerous parameters whose values must be determined through the appropriate experiments. In the absence of such experiments, a sensitivity analysis can shed light on the different aspects of the model on and clarify Li–S cell behavior. To study the physical and mathematical abilities and limits of the model, a wide mathematical range is assumed for the parameters.

The behavior of the model at various discharge current rates was previously studied [9], and the details of the voltage plateaus at each current rate were explained. Furthermore, a sensitivity analysis of the cathode conductivity was performed, demonstrating the existence of an essential threshold of conductivity for a working cell [9]. After discharge, the distribution of the precipitants is not uniform; the degree of this non-uniformity depends on the discharge current rates and cathode conductivity. In addition, the precipitants diffuse in the separator, thus causing a fading cycle life.

* Corresponding author. Tel.: +1 519 888 4567x35586; fax: +1 519 888 4347.
E-mail address: p4chen@uwaterloo.ca (P. Chen).

0378-7753/$ – see front matter © 2014 Elsevier B.V. All rights reserved.
http://dx.doi.org/10.1016/j.jpowsour.2013.12.145

This part of the sensitivity analysis focuses on the rate constants of precipitation and the sulfur content.

2. Model development and governing equations

The model is based on the proposed model by K. Kumaresan, Y. Mikhaylik, and R.E. White [8]. Fig. 1 presents a schematic of the Li–S cell and summarizes the governing equations and boundary conditions of the model. Appendix B describes the model, and Appendix A defines its parameters. The values proposed for the parameters are provided in Tables 1–4 in Appendix C.

The reactions in the cell include Li metal oxidization at the anode surface during discharge [8]:

$$\mathrm{Li} \rightleftharpoons \mathrm{Li}^+ + \mathrm{e}^- \tag{1}$$

It is assumed that during discharge, the elemental sulfur, which is initially in the solid phase, dissolves in the electrolyte and then goes through the following electrochemical reactions [8]:

$$\frac{1}{2}\mathrm{S}_{8(\mathrm{l})} + \mathrm{e}^- \rightleftharpoons \frac{1}{2}\mathrm{S}_8^{2-} \tag{2}$$

$$\frac{3}{2}\mathrm{S}_8^{2-} + \mathrm{e}^- \rightleftharpoons 2\mathrm{S}_6^{2-} \tag{3}$$

$$\mathrm{S}_6^{2-} + \mathrm{e}^- \rightleftharpoons \frac{3}{2}\mathrm{S}_4^{2-} \tag{4}$$

$$\frac{1}{2}\mathrm{S}_4^{2-} + \mathrm{e}^- \rightleftharpoons \mathrm{S}_2^{2-} \tag{5}$$

$$\frac{1}{2}\mathrm{S}_2^{2-} + \mathrm{e}^- \rightleftharpoons 2\mathrm{S}^{2-} \tag{6}$$

The following precipitation/dissolution reactions are also present:

$$\mathrm{S}_{8(s)} \rightleftharpoons \mathrm{S}_{8(l)} \tag{7}$$

$$2\mathrm{Li}^+ + \mathrm{S}_8^{2-} \rightleftharpoons \mathrm{Li}_2\mathrm{S}_{8(\mathrm{s})} \tag{8}$$

$$2\mathrm{Li}^+ + \mathrm{S}_4^{2-} \rightleftharpoons \mathrm{Li}_2\mathrm{S}_{4(\mathrm{s})} \tag{9}$$

$$2\mathrm{Li}^+ + \mathrm{S}_2^{2-} \rightleftharpoons \mathrm{Li}_2\mathrm{S}_{2(\mathrm{s})} \tag{10}$$

$$2\mathrm{Li}^+ + \mathrm{S}^{2-} \rightleftharpoons \mathrm{Li}_2\mathrm{S}_{(\mathrm{s})} \tag{11}$$

The details of the model and its governing equations can be found either in Appendix B or ref. [8]. The current densities due to the electrochemical reactions are given by the Bulter–Volmer equation.

3. Results and discussion

A range of variations is assumed for each parameter. This range is not bounded by a range of physical values. The goal is to determine the behavior of the model system with respect to different situations and to find a range for the parameters in which the Li–S cells are feasible. However, the functionality of the model with respect to these parameters was found not to be linear. Instead, we must choose a parameter each time and investigate the changes in the model from variations in this parameter while keeping the other parameters constant.

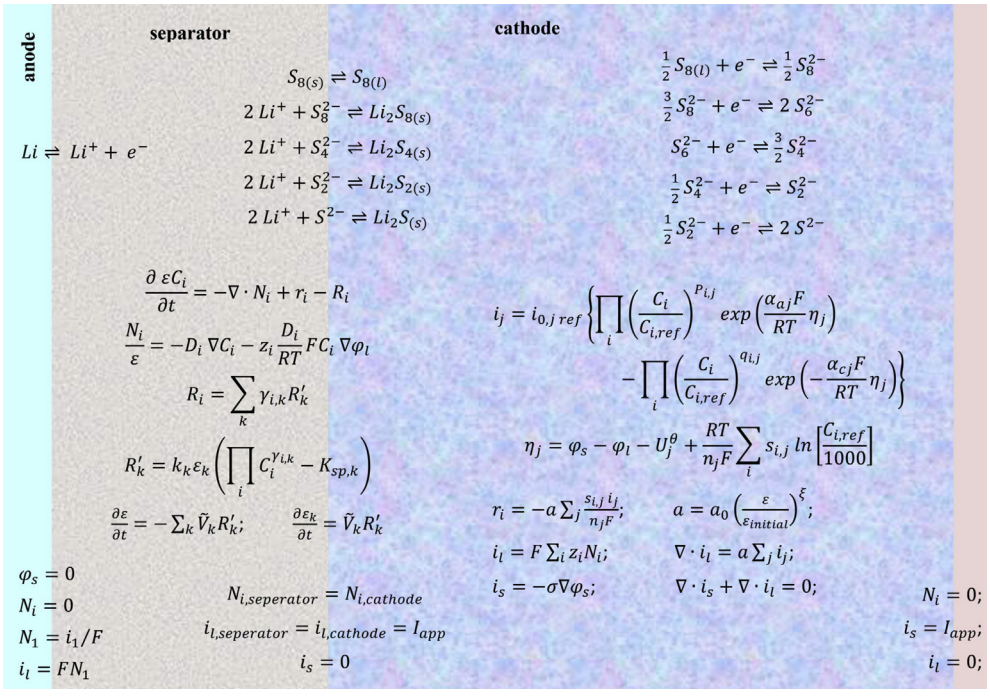

Fig. 1. Schematic of a Li–S cell and a summary of the governing equations and boundary conditions. Repeated from Ref. [9].

The normalized current, due to electrochemical reaction j in the cathode and defined by the following expression [9], is used to illustrate the kinetics of the system:

$$I_j^N = \frac{1}{I_{app}} \int_{x=L_s}^{x=L} a i_j dx \tag{12}$$

where $\sum_{j=2}^{6} I_j^N = 1$. In other words, I_j^N describes the overall contribution of the electrochemical reaction j in producing the discharge current at a given time. In the ideal case of utilizing the entire capacity of sulfur, the discharge normalized currents satisfy the following relations:

$$\frac{1}{T_{DC}} \int_{t=0}^{T_{DC}} I_j^N dt = C_j, \tag{13a}$$

$$\{C_2, \ldots, C_6\} = \left\{\frac{1}{8}, \frac{1}{24}, \frac{1}{12}, \frac{1}{4}, \frac{1}{2}\right\} \tag{13b}$$

where T_{DC} is the total time of an ideal complete discharge and C_j is the portion of reaction j in the total capacity. The responses of the normalized currents with respect to the applied current were discussed in detail in Ref. [9].

3.1. Rate constants for the precipitation reactions

Each rate constant controls the dissolving and precipitating speed of the related species. Although the model predicts that the precipitation rate and dissolution rate behave symmetrically around the saturation concentrations (see Equation (B13)), far away from saturation, they behave differently: there is no limitation on the precipitation rates if the concentration of the species increases, but dissolution rates have an upper limit that depends on the related solubility product, rate constant, and solid volume fraction.

This fact means the precipitated species may not dissolve back into the solution to be involved in the reactions. In the model, an initial equilibrium between the electrochemical reactions and precipitation reactions is assumed; therefore, changes in the solubility products were avoided to conform to this assumption. Numerical instability was observed when this assumption was ignored.

The solubility of each species, and thus their respective rate constants, depends on the solvent used. Because the kinetics of each reaction is influenced by the concentration of each species, the discharge voltage will also depend on the solvent. In this section, the rate constant parameters are the subject of study. Figs. 2 and 3 present the simulation results for 0.1 C and 1 C, respectively.

The behavior for the rate constant of solid elemental sulfur, $k_{S_{8(s)}}$, is simple. If the dissolution speed is fast compared to the reduction rate of $S_{8(l)}$, a two-stage voltage plateau exists. As the rate constant decreases, the $S_{8(l)}$ concentration, and thus the discharge voltage, becomes lower. The first discharge plateau vanishes, and the

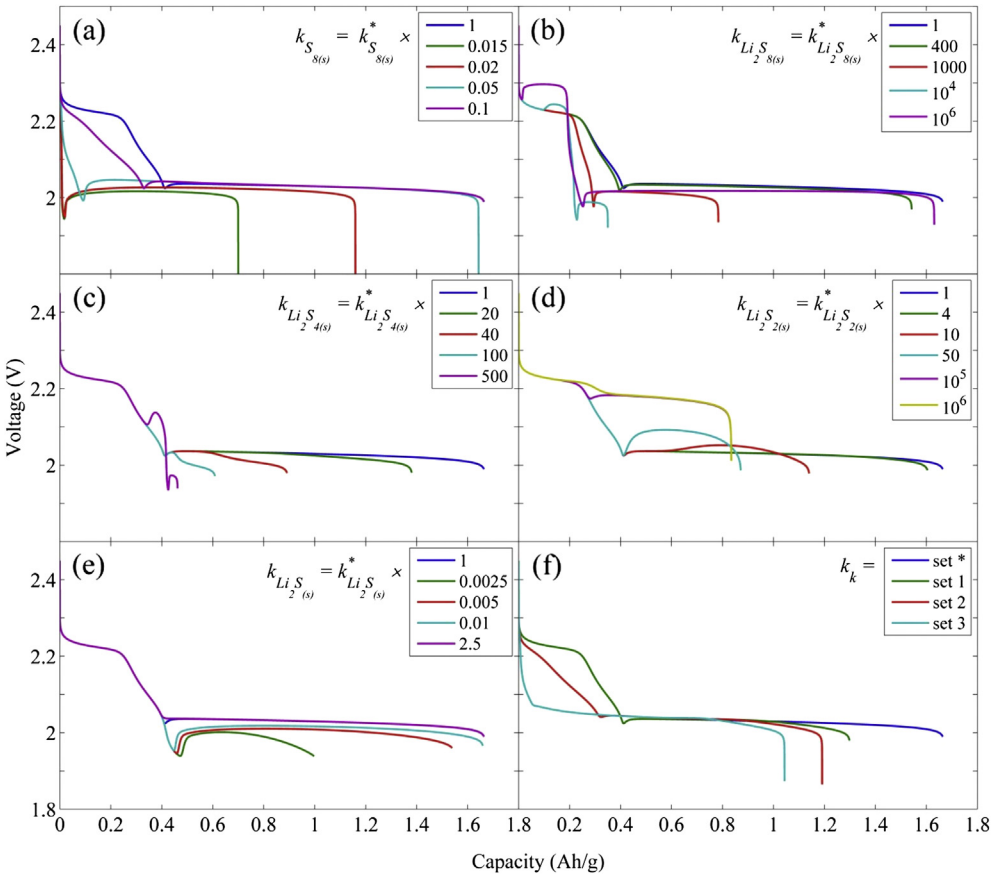

Fig. 2. Discharge voltage plateau for different rate constants at discharge current rates of 0.1 C. (a)–(e) In each case, only the mentioned rate constant differs from the initial assumptions. (f) Some other cases for comparison. In each set, $k_k = k_k^* \times b_k$, and b_k are equal to one in "set*", {1, 1, 20, 6, 1} in "set 1", {0.1, 1, 25, 8, 2.5} in "set 2", and {0.051, 1, 60, 16, 250} in "set 3".

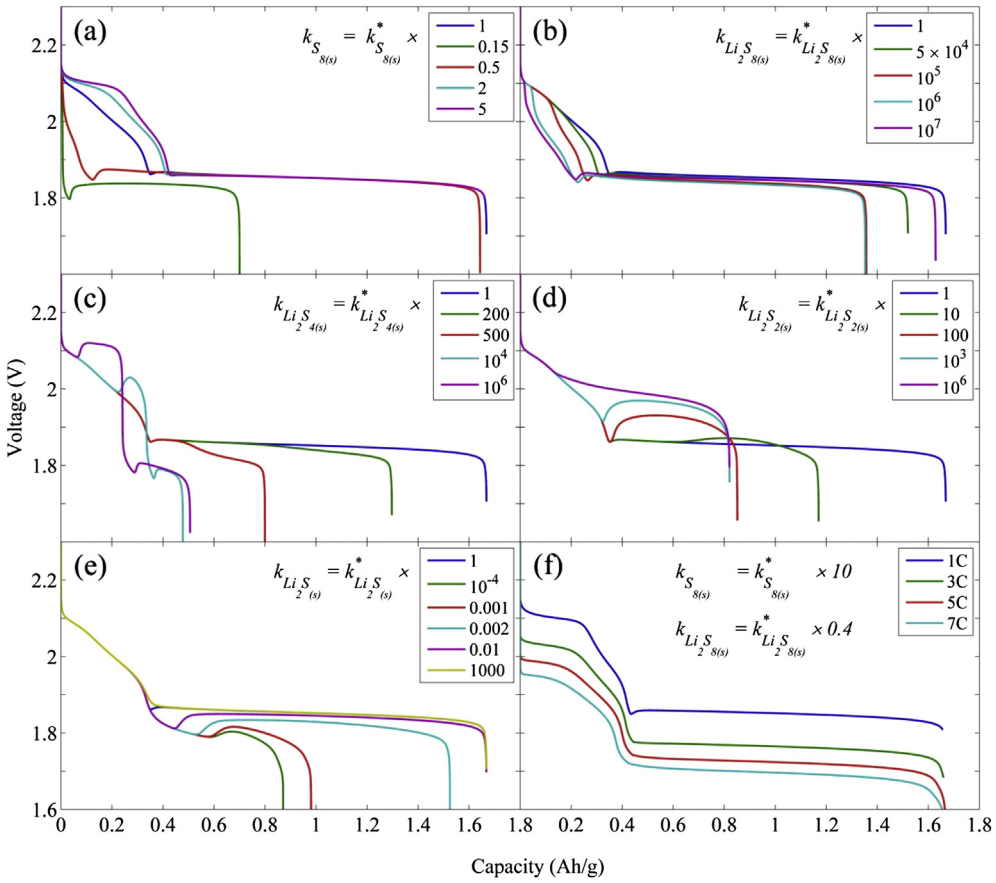

Fig. 3. Discharge voltage plateau for different rate constants at a discharge current rate of 1 C. (a)–(e) in each case, only the mentioned rate constant differs from the initial assumptions. (f) Discharge voltage plateau at high C rates for the case with a high solubility of sulfur.

contribution of the sulfur reduction in the discharge current per time decreases, causing $S_{8(s)}$ to last longer in the system. As expected, for equal ratios of $k_{S_{8(s)}}/I_{app}$, similar behaviors for discharge and retained discharge capacity were observed (Figs. 2a and 3a); only the sharp trough changes due to the different ratio of $k_{Li_2S_{(s)}}/I_{app}$.

For the mid-polysulfide products, the behavior is more complicated, particularly on the voltage plateau. The effect of the rate constant on the capacity can be summarized as follows. To start the precipitation of a species, a rate constant threshold is required, which depends on the concentration of the species and thus the applied current. As rate constant exceeds the threshold to a greater degree, the amount of the solid phase of the species formed becomes greater. As mentioned earlier, rapid precipitation does not necessarily mean rapid dissolution, and the precipitated material is not involved in the electrochemical reaction, thus leading to capacity loss. If the rate constant is sufficiently large to reproduce the amount of species dissolved in the electrolyte, the retention capacity increases again. This type of behavior, over a mathematical range, is observed for $k_{Li_2S_{8(s)}}$ and $k_{S_{8(s)}}$ (Figs. 2b, 3b and 3c).

The voltage plateau behavior depends on more parameters and is more complicated. At 0.1 C, increasing $k_{Li_2S_{8(s)}}$ by a factor of 400 causes the threshold of initiating precipitation to be exceeded, leading to some capacity loss. If the rate constant is increased further, S_8^{2-} will be removed earlier and faster, causing the reduction of $S_{8(l)}$ to increase up to a peak; not the peak of I_3^N will vanish, but the reverse oxidization of S_6^{2-} will make it negative. This phenomenon occurs for $k_{Li_2S_{8(s)}} \geq k^*_{Li_2S_{8(s)}} \times 1000$, causing significant capacity loss.

A factor of 10^4 makes this phenomenon stronger: as precipitation starts, when it passes its peak, I_2^N becomes one and the voltage increases, i.e., a new type of deep trough forms. Although precipitation has started, the S_8^{2-} concentration remains constant while all of the elemental sulfur reduces. With a decrease in the concentration of $S_{8(l)}$, the potential also decreases, and some of the S_8^{2-} will be reduced. Only a small portion of sulfur will reduce to S^{2-}, and most of the capacity will be lost.

At $k_{Li_2S_{8(s)}} = k^*_{Li_2S_{8(s)}} \times 10^6$, almost all of the capacity can be maintained. Precipitated materials dissolve again, contributing in electrochemical reactions.

A higher rate constant threshold is expected at 1 C. Interestingly, the lowest maintained capacity is much higher than 0.1 C, and the potential in the first plateau always decreases. The key is the lower dissolution rate of elemental sulfur with respect to the electrochemical reaction rates. The $S_{8(l)}$ concentration is always low, and I_2^N cannot become one; therefore, the voltage of the first plateau reduces. In contrast, the S_8^{2-} concentration does not considerably exceed saturation, leading to slow precipitation compared to the electrochemical reaction rate. Particularly after a period of time, because the S_8^{2-} production rate is low, its concentration remains below saturation, even causing the precipitated material to redissolve in the electrolyte. Therefore, a cell discharges more even for the same ratios of $k_{Li_2S_{8(s)}}/I_{app}$.

The same explanation applies to the $k_{Li_2S_{4(s)}}$ parameter as well. If this rate constant is increased, active material is lost by precipitation. Eventually, an increase in this rate allows for re-dissolution, thus retaining more capacity. S_4^{2-} precipitation lowers its concentration, causing a decrease in potential along with a local minimum

in I_5^N and I_6^N, whereas I_4^N presents a peak. The decrease in potential allows for the semi-equilibrium of reaction rates.

At 0.1 C, only for $k^*_{Li_2S_{4(s)}} \times 500$ does S_4^{2-} precipitation occur before the second plateau, leading to another deep trough in the potential. At this point, the reduction of S_4^{2-} has not yet started. As the S_4^{2-} concentration decreases due to precipitation, less overpotential is required to reduce S_6^{2-} and the potential increases, leading to faster S_6^{2-} reduction and also to its partial reverse oxidization and the partial reverse oxidation of S_8^{2-}. The increased potential leads to a new semi-equilibrium between the electrochemical reactions (I_2^N, I_3^N and I_4^N) until the S_6^{2-} concentration decreases very suddenly, which causes a sudden decrease in potential. The same behavior is observed at 1 C.

At a rate constant increased by factors of 10^4 and 10^6, precipitation again occurs in the first plateau, causing another deep trough. At factors of 10^6 and higher, the discharge capacity starts to increase again.

Increasing $k_{Li_2S_{2(s)}}$ increased the amount of S_2^{2-} precipitation. As the constant rate becomes larger, the precipitation becomes faster and the S_2^{2-} concentration decreases. Therefore, the potential increases along with an increase in I_5^N and a decrease in I_6^N. At $k^*_{Li_2S_{2(s)}} \times 50$, the precipitation of S_2^{2-} and S^{2-} both begin simultaneously (see Fig. 2d). I_5^N increases to a very large peak, and with an increase in the potential, reverse oxidation of S_4^{2-} occurs, with I_6^N becoming almost zero after a sharp and relatively small peak. Only a small portion of S_2^{2-} reduces to S^{2-}.

Increasing the rate constant by a factor greater than 50 causes the precipitation to start before the second plateau. Consequently, the factors of 10^5 and 10^6 cause a large increase in the potential, and no reduction of S_2^{2-} occurs. Therefore, only half of the capacity is maintained.

The same behavior is observed at 1 C (see Fig. 3d). For the same ratios of $k_{Li_2S_{2(s)}}/I_{app}$, the same discharge capacity is retained. Attempts to increase the discharge capacity by increasing the rate constant failed because of numerical instability.

The precipitation of the last polysulfide, S^{2-}, is controlled by $k_{Li_2S_{(s)}}$. Removing the last product from the electrolyte is necessary to fully discharge the cell and to avoid the cost of decreasing voltage due to high product concentration. As long as the rate constant is above a threshold (which depends on the applied current), the product removal occurs perfectly and no change in the shape or behavior occurs (see the largest values of the rate constant in Figs. 2e and 3e).

At 0.1 C, the only difference in the discharge plateau between the two highest values of the rate constant is the lack of the trough (also in 1 C, see Fig. 3e). At high values of the rate constant, as soon as S_2^{2-} reduction begins, S^{2-} product begins to precipitate because very tiny solid phase nuclei can initiate the precipitation. However, at $k^*_{Li_2S_{(s)}}$, the tiny nuclei cannot initiate the precipitation, so the S^{2-} concentration exceeds the saturation point and the potential decreases until the very sudden start of precipitation removes the product, at which point the potential increases.

Decreasing the rate constant by a factor of 0.01 delays the precipitation, which causes the accumulation of S^{2-} in the electrolyte, thereby resulting in a further decrease in the potential. The lower potential causes enhanced production of S_2^{2-} as well, such that it starts to precipitate; however, the precipitation does not last long because S^{2-} suddenly starts to precipitate. The removal of S^{2-} brings the potential back to a higher level, along with a very large peak of S_2^{2-} reduction, its reverse oxidization to S_4^{2-}, and even reverse oxidization to S_6^{2-}. As the rate constant continues to decrease, the precipitation becomes more delayed and these effects become stronger.

At $k^*_{Li_2S_{(s)}} \times 0.0025$, most of the precipitated species are $Li_2S_{2(s)}$; therefore, the discharge capacity only just exceeds half of the total capacity. Note that as the S_4^{2-} concentration (and also S_6^{2-}) decreases due to electrochemical reactions and most of the S_2^{2-} is removed by precipitation and not by the electrochemical reactions (the contribution of I_6^N in total current is weak), the potential gradually decreases to maintain the reduction of S_4^{2-}.

The same behavior is observed at 1 C, except that the deep trough is stretched in its time scale (Fig. 3e). This stretching occurs because when the reduction of both S_4^{2-} and S_2^{2-} begins, elemental sulfur and the high polysulfides are still being reduced as well (whereas at 0.1 C, no significant reduction of the high polysulfides occurs because they are all consumed; see Fig. 3 in Ref. [9]). Therefore, I_5^N is not as high as in the 0.1 C case; as a result, on the time scale of the 1 C case, the precipitation is delayed longer, thereby leading to the stretched trough. When the rate constant is decreased by a factor of 0.002 or lower, S_2^{2-} precipitation also occurs. At the factor of 0.001, S_2^{2-} precipitation starts slightly before S^{2-} precipitation and constitutes the major solid phase. Decreasing the rate constant by a factor of 10^{-4} causes all of the precipitation to be $Li_2S_{2(s)}$ instead of $Li_2S_{(s)}$, resulting in a discharge of only half of the capacity.

Three representative cases are presented in Fig. 2f to emphasize the nonlinear behavior of the system. In each set, $k_k = k_k^* \times b_k$ and b_k are equal to one in "set*", {1, 1, 20, 6, 1} in "set 1", {0.1, 1, 25, 8, 2.5} in "set 2", and {0.051, 1, 60, 16, 250} in "set 3". The only difference between the discharge plateau of "set*" and "set 1" is the shorter second plateau. The higher rate constants for $Li_2S_{4(s)}$ and $Li_2S_{2(s)}$ cause the loss of capacity. At the end of the discharge, the volume fractions are approximately 0.037 and 0.025 for $\varepsilon_{Li_2S_{2(s)}}$ and $\varepsilon_{Li_2S_{4(s)}}$, respectively. $\varepsilon_{Li_2S_{(s)}}$ drops from approximately 0.287 in "set*" to 0.183 in "set 1". In "set 2", decreasing $k_{S_{8(s)}}$ by a factor of 0.1 makes the first discharge plateau similar to that at the 1 C discharge rate (see Fig. 3). However, the three last rate constants lead to a significant capacity loss. Note that the second plateau remains fairly flat. The volume fractions are approximately 0.039, 0.037, and 0.159 for $\varepsilon_{Li_2S_{4(s)}}$, $\varepsilon_{Li_2S_{2(s)}}$, and $\varepsilon_{Li_2S_{(s)}}$, respectively. "Set 3" indicates how the rate constants allow only one discharge plateau to occur.

A comparison of different discharge rates for the cell with high solubility is shown in Fig. 3f. Even for a very high rate of 7 C, all of the capacity is retained. The two plateaus are easily distinguishable. In addition, the sharp curves become smooth, particularly those in the deep trough that disappeared. The reason for this behavior is the dependency of dissolution on the size of the particle; for high C rates, as sulfur particles become smaller, they dissolve slower than the rate of the electrochemical reactions, thus causing a smooth start and end for each electrochemical reaction and thus a smooth increase or decrease of the concentrations of the species. Consequently, S^{2-} starts to precipitate gradually, not suddenly, and the trough disappears.

The location of the precipitated material is very important. If the rate constant is high, the species precipitate inside the cathode. However, if the rate constant is small, the dissolved species diffuses into the separator and precipitates there as well. To illustrate this effect, the volume fraction of $Li_2S_{(s)}$ is presented in Fig. 4, which demonstrates that a further decrease in the rate constant leads to an increase in the formation of the solid phase in the separator. Such movement of the active material to the separator is a cause of capacity fading by cycling. Considering the possibility of higher-polysulfide precipitation makes this fading effect even worse. For example, Fig. 5 shows the volume fraction of $Li_2S_{2(s)}$ and $Li_2S_{(s)}$ across the cell at the end of a discharge. The low rate constant of $k_{Li_2S_{2(s)}}$ leads to a uniform precipitation across the entire cell. However, a large rate constant leads to the presence of more solid phase everywhere compared to the case of a low rate constant, but not distributed uniformly. The volume fraction is higher in the

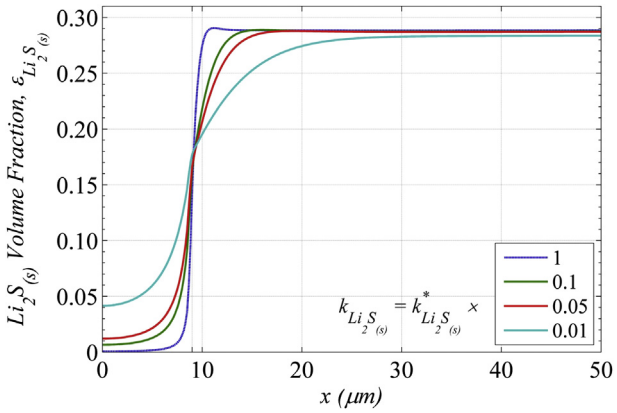

Fig. 4. Volume fraction of $Li_2S_{(s)}$, $\varepsilon_{Li_2S_{(s)}}$ across the cell at the end of a discharge with a discharge current rate of 0.1 C. The separator–cathode interface is located at $x = 9$ μm.

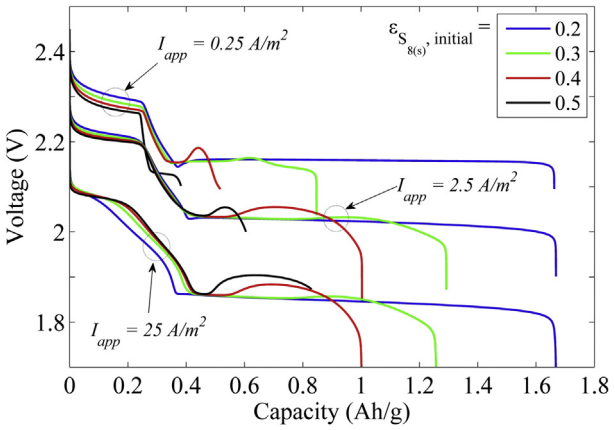

Fig. 6. Discharge plateaus with different sulfur volume content at various discharge current rates.

cathode. The dynamics of precipitation was discussed earlier in Ref. [9].

3.2. Sulfur content

It is desirable to increase the energy density of a battery by increasing the active material content per volume of the cathode. The volume expansion of the sulfur products during the discharge processes and the porosity loss are limitations that place an upper limit for the sulfur content. This section provides a quantitative discussion of the cell behavior with respect to the sulfur content based on the discharge current rate. Note that based on the model, the entire cathode-electrolyte interface is considered to be an active surface for electrochemical reactions, thus ignoring the insulating nature of sulfur and the precipitated polysulfides. Therefore, the negative phenomenon of losing active surface area for electrochemical reactions is not considered. For simplicity, the volume ratio of conductive material in a cathode and its structure (porosity and specific surface area) are assumed to remain constant even if the sulfur content is changed.

Simulations were performed at the three different discharge current rates of 0.25, 2.5, and 25 A m^{-2}. Fig. 6 presents the discharge plateaus for various sulfur content levels, and Fig. 7 presents the retained discharge capacity as a function of sulfur content. Both of the figures indicate that cells with less than 20% sulfur content (per volume of cathode) can be fully discharged, even for high discharge rates of approximately 1 C. At a high discharge current rate of 25 A m^{-2}, the short first plateau and a vanishing trough is expected, as explained earlier.

When the sulfur content is 0.3, at higher discharge rates, the voltage plateaus are very similar to those in Figs. 2d and 3d when $Li_2S_{2(s)}$ forms, whereas at 0.25 A m^{-2}, the discharge rate is similar to that in the plateaus with S_4^{2-} precipitation (see Figs. 2c and 3c). At a discharge rate of 25 A m^{-2}, if the sulfur content exceeds 30% of the cathode volume, the first discharge plateau attains its full shape because $\varepsilon_{S_{8(s)}}$ is sufficiently large to keep the dissolution sufficiently fast for a relatively longer time. An almost constant $S_{8(l)}$ concentration is obtained, and consequently, a sufficiently high S_8^{2-} concentration in the electrolyte (as the reduction product of elemental sulfur) is achieved, and thus, no potential reduction is required to involve S_8^{2-} in the electrochemical reaction. Although with the sulfur content of 0.4, the voltage plateaus at high discharge rates are similar to those in previous simulation results; at low discharge rates, the voltage plateau has an unexpected shape and end. For a sulfur content of 0.5, all of the discharges are observed to stop in a manner that is not regulated until the end of the electrochemical reactions.

Fig. 7 provides more details of the discharge capacity. For a low discharge rate, the discharge capacity percentage decreases rapidly

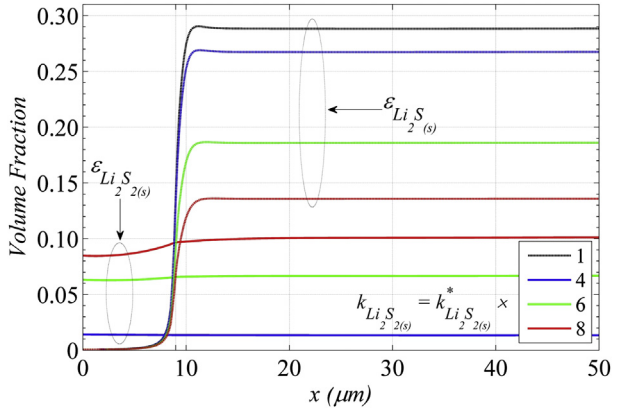

Fig. 5. Volume fraction of $Li_2S_{(s)}$ ($\varepsilon_{Li_2S_{(s)}}$) and $Li_2S_{2(s)}$ across the cell at the end of a discharge with a discharge current rate of 0.1 C. The separator–cathode interface is located at $x = 9$ μm.

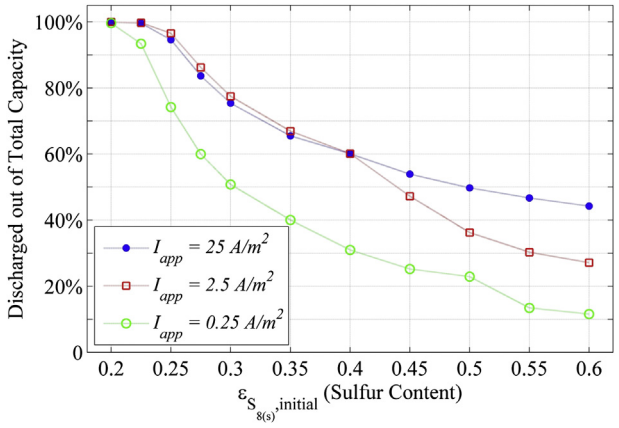

Fig. 7. Discharge capacity percentage out of the total capacity for the cells with different sulfur contents and at various discharge rates.

because the reduction reactions of the different polysulfides occur more individually, i.e., a polysulfide almost reduces completely before the products start the subsequent reaction. Therefore, the concentration of high polysulfides can reach the saturation concentration and begin to precipitate. At a discharge rate of 0.25 A m^{-2}, even a sulfur content of 0.225 increases the S_4^{2-} concentration to the saturation point such that $\varepsilon_{Li_2S_{4(s)}}$ at the cathode area is almost 0.02 on average. This volume fraction increases to approximately 0.334 when the sulfur content is 0.4, whereas $\varepsilon_{Li_2S_{(s)}}$ decreases to approximately 0.06.

Increasing the sulfur content by over 0.4 causes a $Li_2S_{8(s)}$ solid phase to form. This solid phase has a sudden increase for a sulfur content of over 0.45, reaching an amount of approximately 0.27 at a sulfur content of 0.5. Thus, the capacity decreases at this point. When the sulfur content is 0.55, all of the solid phase is $Li_2S_{8(s)}$, and even for 0.6, approximately 0.07 of the sulfur volume fraction remains in the cathode without being involved in the reactions. For all of these sulfur content levels, only an insignificant amount of solid $Li_2S_{2(s)}$ forms because of the simultaneous reduction of S_4^{2-} and S_2^{2-}, which prevents the S_2^{2-} concentration to reach the saturation point. In the previous section, high polysulfides were shown to precipitate everywhere in the cell. Large amounts of precipitated material can block the cathode-separator interface. At a discharge current rate of 0.25 A m^{-2}, this blocking phenomenon occurs for cells with a sulfur content of 0.4 and greater.

At high discharge current rates, partially simultaneous reduction of the different polysulfides prevents the saturation of one specific high polysulfide that causes higher capacity retention with respect to the low discharge currents. At a discharge rate of 2.5 A m^{-2}, the major solid phase changes from $Li_2S_{(s)}$ to $Li_2S_{2(s)}$ by increasing the sulfur content up to 0.4 ($Li_2S_{(s)}$ and $Li_2S_{2(s)}$ become approximately 0.162 and 0.354, respectively). However, a very small amount of $Li_2S_{4(s)}$ forms when the sulfur content is 0.4 (approximately 0.02), but increasing the sulfur content to 0.45 increases its volume fraction suddenly (approximately 0.12), which causes an even greater reduction in the discharge capacity. The details of the average volume fractions of the precipitants in the cathode area are provided in Fig. 8. At this point, the cathode-separator interface becomes blocked as well. The higher sulfur content leads to an increase in the $Li_2S_{4(s)}$ precipitates. The precipitated material almost completely fills the pores of the separator (the porosity becomes less than 0.05 in the separator at a sulfur content of 0.6) and blocks the cathode-separator interface.

At a high discharge rate of 25 A m^{-2}, no solid phase of $Li_2S_{4(s)}$ forms, resulting in the smooth blue line (in web version) in Fig. 7. For sulfur contents greater than 0.4, the cathode-separator interface is blocked. The slightly lower discharge capacity at $I_{app} = 25$ A m^{-2} compared to 2.5 A m^{-2}, when the sulfur content is between 0.225 and 0.4, is related to the relatively earlier appearance of S_2^{2-} at the higher current rates, which causes slightly more precipitation.

To find the optimum sulfur content to gain the highest capacity of the cell, the discharge capacity per surface area of the cathode is presented in Fig. 9. The optimum sulfur content is between 0.225 and 0.25, depending on the discharge current. However, considering the movement of active material to the separator due to the precipitation of $Li_2S_{n\geq 2}$ precipitations, one should keep the sulfur content below 0.225 to avoid poor cyclability.

The shapes of the curves in the graphs shown in Figs. 7 and 9 suggest a way to distinguish the precipitant as the final product of the discharge process. Each of the points in the figure which exhibits a sudden decrease in the line that indicates the discharge capacity is related to the initiation of the precipitation of the species.

Note that these results depend on the coefficients of the precipitation rate constants, particularly the shape of the voltage plateaus. However, the result that at high sulfur contents, a higher discharge capacity is observed at high discharge rates, unlike at low discharge rates, is a direct consequence of the assumed chain of reduction, meaning that other sets of rate constants exhibit the same results. At low discharge rates, the reduction of the various species does not occur simultaneously, thus leading to the saturation of high polysulfides.

In carbon-sulfur composite cathodes, as one of the most popular methods for cathode preparation, the melt sulfur (or dissolved to a solvent) diffuses into the porous structure of carbon [3,10]. Therefore, theoretically, the morphology of carbon structure does not significantly change. The ratio of carbon/sulfur only determines the ratio of sulfur volume to pore volume without remarkable change in the conductivity of carbon matrix. In this case, the behavior of the system follows the results of this section on sulfur content. However, high amounts of sulfur may disconnect carbon particles and cause to decrease in the effective conductivity of carbon matrix. B. Zhang et al. have reported loss of specific capacity by increasing the sulfur content [10]. They used melted sulfur diffusion into micropores of carbon. In other methods of preparation for carbon-

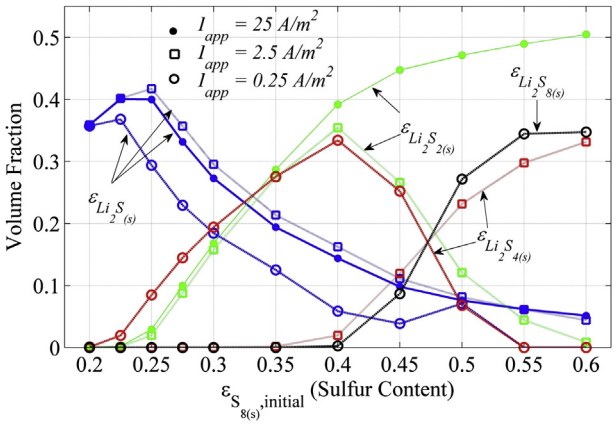

Fig. 8. Average volume fraction of precipitants across the cathode at the end of a discharge for different discharge current rates.

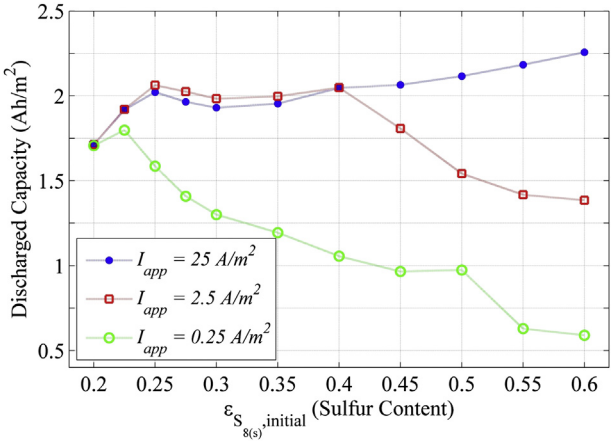

Fig. 9. Discharge capacity per unit surface area of the cathode for different sulfur contents and at various discharge rates.

sulfur cathodes, such as mixing [3] or carbon coating on a surface of sulfur cathode [11], the morphology of the carbon matrix may changes by different ratios of carbon/sulfur. However, through this change of morphology, the available surface area of carbon matrix may not change considerably; the conductivity of carbon matrix is subjected to most significant change. Increasing carbon contents directly increases the conductivity of the cathode. We have discussed the importance of conductivity of the cathode in detail in Part I [9].

4. Conclusions

In this paper, the behavior of a Li–S cell mathematical model was investigated with respect to a wide mathematical range of rate constants for precipitation reactions. The dissolving speed of elemental sulfur was observed to determine whether the discharge voltage has either one or two plateaus: more rapid dissolution than consumption by electrochemical reaction causes the two flat regions. In fact, k_k/I_{app} plays an important role in the behavior of the cell and its capacity. However, the model indicates a strong nonlinear behavior with respect to this ratio. More specifically, there is a "critical interval" for each rate constant, in which a tiny variation in the rate constant causes a large variation in the response of a cell, particularly in its capacity. The existence of these critical intervals suggests that the model requires modification in its formulating of the precipitation reactions.

Moreover, the model fails to reproduce the voltage plateau of the cases with capacity loss. In such cases, the final products in the cathode should consist of $Li_2S_{(s)}$, $Li_2S_{2(s)}$, and $Li_2S_{4(s)}$, and some unutilized sulfur should remain as well. Forcing the model to reflect this situation reforms the voltage plateau into shapes that cannot be compared with the experiment results. In other words, regardless of how well the model works in simulating a perfect battery that retains full capacity, it fails in the simulations of typical batteries that lose capacity. However, the model still provides a considerable amount of valuable information. For example, the model indicates that for slow precipitation, more material diffuses to the separator, leading to a decreased cycle life. Specifically, this decreased cycle life phenomenon is stronger if the precipitant is one of the high polysulfides.

Most of the phenomena in a cell, which are ignored in the model (such as the isolating nature of sulfur and polysulfides), can reduce the predicted discharge capacity; therefore, the model is also used to determine an upper limit on the optimal sulfur content. For low discharge rates, the model predicts that the discharge capacity percentage reduces rapidly by increasing the sulfur content compared to that at high rates. This phenomenon is related to the assumed sequence of the reduction reactions chain. Thus, some modification to this assumption should be implemented in future models.

Unfortunately, all attempts to charge the modeled cell failed due to a low saturation concentration of $Li_2S_{(s)}$ in the electrolyte. This fact indicates that modifications to the model are necessary.

Acknowledgments

Financial support for this work was provided by Positec, the Natural Sciences and Engineering Research Council of Canada (NSERC), Canada Foundation for Innovation (CFI), and the Canada Research Chairs (CRC) program. The authors are grateful to The Nam Long Doan for very useful discussions.

Appendices

A. Parameters and symbols (primarily taken from ref. [5])

a	specific surface area of the cathode
a_0	initial value of a
b	Bruggeman coefficient
c_i	concentration of species i ($i = Li^+, S_{8(l)}, S_8^{2-}, S_6^{2-}, S_4^{2-}, S_2^{2-}, S^{2-}$, and A^- (anion of the lithium salt used in the electrolyte)), mol m^{-3}
$c_{i,ref}$	reference concentration of species i, mol m^{-3}
C_j	portion of reaction j in the total capacity for an ideal complete discharge
$D_{i,0}$	diffusion coefficient of species i in the bulk medium, m^2 s^{-1}
D_i	diffusion coefficient of species i in the porous medium, m^2 s^{-1}
F	Faraday constant, C equi^{-1}
i_j	current density due to reaction j, A m^{-2}
$i_{j,ref}$	exchange current density of the electrochemical reaction j at the reference concentrations, A m^{-2}
i_l	superficial current density in the liquid phase, A m^{-2}
i_s	superficial current density in the solid phase, A m^{-2}
I_{app}	applied current density, A m^{-2}
I_j^N	normalized current due to electrochemical reaction j
$K_{sp,k}$	solubility product of precipitate k
k_k	rate constant of precipitate k
L	thickness of the cell, m
L_s	thickness of the separator, m
N_i	superficial flux of species i, mol m^2 s^{-1}
n_j	number of electrons transferred in electrochemical reaction j
$p_{i,j}$	anodic reaction order of species i in electrochemical reaction j
$q_{i,j}$	anodic reaction order of species i in electrochemical reaction j
R	gas constant, J mol^{-1} K^{-1}
R_i	production rate of species i due to precipitation reactions, mol m^3 s^{-1}
$R_k^{'}$	rate of precipitation of solid species k, mol m^3 s^{-1}
r_i	production rate of species i due to electrochemical reactions, mol m^3 s^{-1}
$s_{i,j}$	stoichiometric coefficient of species i in electrochemical reaction j
T	temperature, K
T_{DC}	Total time of an ideal complete discharge, s
t	time, s
U_j^θ	Standard Open Circuit Potential (OCP) of electrochemical reaction j
$U_{j,ref}$	OCP of electrochemical reaction j at reference concentrations, V
$\tilde{V}_k$	molar volume of the precipitate k, m^3 mol^{-1}
z_i	charge number of species i
α_{aj}	anodic transfer coefficient of reaction j
α_{cj}	cathodic transfer coefficient of reaction j
ε	porosity of the separator and cathode
ε_k	volume fraction of precipitate k in the separator and cathode
φ_l	Potential in the liquid phase, V
φ_s	Potential in the solid phase, V
$\gamma_{i,k}$	number of ionic species i produced by dissociation of precipitate k
η_j	overpotential for electrochemical reaction j

σ effective conductivity of the solid phase of the cathode, $N_i = 0$

ξ morphology parameter

B. Governing equations

The model includes the electrochemical reactions given by Equations (1)–(6) and the precipitation/dissolution reactions given by Equations (7)–(11). In a porous medium, the governing equation for the material balance of an individual species is

$$\frac{\partial \varepsilon C_i}{\partial t} = -\nabla \cdot N_i + r_i - R_i \tag{B1}$$

where the flux is given by

$$\frac{N_i}{\varepsilon} = -D_i \nabla C_i - z_i \frac{D_i}{RT} F C_i \nabla \varphi_l \tag{B2}$$

The diffusion coefficient for species i, D_i, is corrected based on Bruggeman's expression for porosity and tortuosity: $D_i = D_{i,0}\varepsilon^b$. The rate of production/consumption of species i due to the electrochemical reactions can be written in the form

$$r_i = a \sum_j \frac{s_{ij} i_j}{n_j F} \tag{B3}$$

where the stoichiometric coefficients are given in Table 1, Appendix C. The specific surface area of the cathode varies due to the precipitation/dissolution of the various lithium sulfide species and is assumed to be governed by the empirical expression:

$$a = a_0 \left(\frac{\varepsilon}{\varepsilon_{\text{initial}}} \right)^{\xi} \tag{B4}$$

where the empirical parameter, ξ, is assigned a value of 1.5. The Butler–Volmer equation yields the current density due to the electrochemical reactions:

$$i_j = i_{0,\text{jref}} \left\{ \prod_i \left(\frac{C_i}{C_{i,\text{ref}}} \right)^{P_{i,j}} \exp\left(\frac{\alpha_{aj} F}{RT} \eta_j \right) - \prod_i \left(\frac{C_i}{C_{i,\text{ref}}} \right)^{q_{i,j}} \times \exp\left(-\frac{\alpha_{cj} F}{RT} \eta_j \right) \right\} \tag{B5}$$

where the overpotential for the reaction j is

$$\eta_j = \varphi_s - \varphi_l - U_{j,\text{ref}} \tag{B6}$$

The terms $p_{i,j} = s_{ij}$ refer to anodic species and $q_{i,j} = -s_{ij}$ refer to cathodic species. The open-circuit potential for reaction j is given by

$$U_{j,\text{ref}} = U_j^{\theta} - \frac{RT}{n_j F} \sum_i s_{i,j} \ln\left[\frac{C_{i,\text{ref}}}{1000} \right] \tag{B7}$$

The liquid phase current density is given by

$$i_l = F \sum_i z_i N_i \tag{B8}$$

The solid phase current density follows Ohm's law

$$i_s = -\sigma \nabla \varphi_s \tag{B9}$$

Because the charge can enter or leave the liquid phase only by electrochemical reactions, the following equations apply at the liquid/solid interface:

$$\nabla \cdot i_l = a \sum_j i_j \tag{B10}$$

and

$$\nabla \cdot i_s + \nabla \cdot i_l = 0 \tag{B11}$$

The rate of consumption or production of species i due to precipitation/dissolution is related to the rate of precipitation/dissolution reaction k by

$$R_i = \sum_k \gamma_{i,k} R'_k \tag{B12}$$

where the rate of precipitation of solid species k is assumed to be governed by the following kinetic equation:

$$R'_k = k_k \varepsilon_k \left(\prod_i C_i^{\gamma_{i,k}} - K_{sp,k} \right) \tag{B13}$$

The volume fraction of the precipitate, k, is a function of time and is given by

$$\frac{\partial \varepsilon_k}{\partial t} = \tilde{V}_k R'_k \tag{B14}$$

Therefore, the porosity variation with time is

$$\frac{\partial \varepsilon}{\partial t} = -\sum_k \tilde{V}_k R'_k \tag{B15}$$

The boundary conditions of the model are as follows. At the interface of the cathode and the current collector, $x = L$, the BCs are

$$N_i = 0 \tag{B16a}$$

$$i_s = I_{\text{app}} \tag{B16b}$$

$$i_l = 0 \tag{B16c}$$

At the cathode-separator interface, $x = L_s$,

$$N_{i,\text{seperator}} = N_{i,\text{cathode}} \tag{B17a}$$

$$i_{l,\ \text{seperator}} = i_{l,\text{cathode}} = I_{\text{app}} \tag{B17b}$$

$$i_s = 0 \tag{B17c}$$

At the surface of anode, $x = 0$,

$$\varphi_s = 0 \tag{B18a}$$

$$N_i = 0 \tag{B18b}$$

$$N_1 = i_1/F \tag{B18c}$$

$$i_l = FN_1 \tag{B18d}$$

The governing equations can be solved numerically.

C. Parameter tables for reference values

Table 1
Stoichiometric coefficients, S_{ij} [8].

S_{ij}	Reactions given by equation (j)					
Species (i)	1	2	3	4	5	6
Li^+	−1	0	0	0	0	0
$S_{8(l)}$	0	−1/2	0	0	0	0
S_8^{2-}	0	1/2	−3/2	0	0	0
S_6^{2-}	0	0	2	−1	0	0
S_4^{2-}	0	0	0	3/2	−1/2	0
S_2^{2-}	0	0	0	0	1	−1/2
S^{2-}	0	0	0	0	0	1
A^-	0	0	0	0	0	0

Table 2
Kinetic and thermodynamic properties [8].

Reaction (j)	$i^*_{0,j\text{ref}}$ (A m^{-2})	α^*_{aj}	α^*_{cj}	n_j	U^θ_j
1	0.394	0.5	0.5	1	0.0
2	1.9719	0.5	0.5	1	2.39
3	0.019719	0.5	0.5	1	2.37
4	0.019719	0.5	0.5	1	2.24
5	1.972×10^{-4}	0.5	0.5	1	2.04
6	1.972×10^{-7}	0.5	0.5	1	2.01

Table 3
Transport properties and reference concentrations [8].

Species (i)	z_i	D^*_{i0} (m^2 s^{-1})	$C^*_{i,\text{ref}}$ (mol m^{-3})
Li^+	+1	1×10^{-10}	1001.08
$S_{8(l)}$	0	10×10^{-10}	19.0
S_8^{2-}	−2	6×10^{-10}	0.1832
S_6^{2-}	−2	6×10^{-10}	0.3351
S_4^{2-}	−2	1×10^{-10}	0.02146
S_2^{2-}	−2	1×10^{-10}	5.999×10^{-7}
S^{2-}	−2	1×10^{-10}	9.94×10^{-10}
A^-	−1	4×10^{-10}	1000

Table 4
Separator and cathode parameters [8].

Parameter	Separator	Cathode
Thickness (m)	9×10^{-6}	41×10^{-6}
$\varepsilon_{\text{initial}}$	0.37	0.778
$\varepsilon_{S_{8(s)},\text{initial}}$	1×10^{-12}	0.160
$\varepsilon_{Li_2S_{8(s)},\text{initial}}$	1×10^{-6}	1×10^{-6}
$\varepsilon_{Li_2S_{4(s)},\text{initial}}$	1×10^{-6}	1×10^{-6}
$\varepsilon_{Li_2S_{2(s)},\text{initial}}$	1×10^{-6}	1×10^{-6}
$\varepsilon_{Li_2S_{(s)},\text{initial}}$	1×10^{-7}	1×10^{-7}
a_0	–	132,762

Table 5
Parameters for the precipitation reactions, either assumed or from Ref. [8].

Precipitate (k)	Rate constant (k^*_k)	Solubility product (K^*_k)	Molar volume ($\tilde{V}_k$(m^{3}mol^{-1}))
$S_{8(s)}$	1.0 s^{-1}	19.0 mol m^{-3}	1.239×10^{-4}
$Li_2S_{8(s)}$	1×10^{-11} m^6 mol^2 s^{-1}	183400 mol^3 m^{-3}	1.361×10^{-4}
$Li_2S_{4(s)}$	9.98×10^{-12} m^6 mol^2 s^{-1}	21480 mol^3 m^{-3}	7.415×10^{-5}
$Li_2S_{2(s)}$	9.98×10^{-9} m^6 mol^2 s^{-1}	0.6006 mol^3 m^{-3}	4.317×10^{-5}
$Li_2S_{(s)}$	6.875×10^{-5} m^6 mol^2 s^{-1}	9.95×10^{-4} mol^3 m^{-3}	2.768×10^{-5}

References

[1] B. Ellis, K.T. Lee, L.F. Nazar, Chem. Mater. 22 (2010) 691–714.
[2] Sheng S. Zhang, J. Power Sources 231 (2013) 153–162.
[3] Xiulei Ji, Linda Nazar, J. Mater. Chem. 20 (2010) 9821–9826.
[4] D.H. Han, et al., J. Electrochem. Soc. 151 (9) (2004) E283–E290.
[5] C. Barchasz, et al., Anal. Chem. 84 (2012) 3973–3980.
[6] V.S. Kolosnitsyn, E.V. Karaseva, Russ. J. Electrochem. 44 (5) (2008) 506.
[7] Y.V. Mikhaylik, Akridge, J. Electrochem. Soc. 151 (11) (2004) A1969.
[8] K. Kumaresan, Y. Mikhaylik, R.E. White, J. Electrochem. Soc. 155 (8) (2008) A576.
[9] M. Ghaznavi, P. Chen, J. Power Sources 257 (2014) 394–401.
[10] B. Zhang, X. Qin, G.R. Li, X.P. Gao, Energy Environ. Sci. 3 (2010) 1531–1537.
[11] Y.J. Choi, et al., J. Power Sources 184 (2009) 548.